NUMERICAL ANALYSIS OF A HYPERSONIC TURBULENT AND LAMINAR FLOW USING A COMMERCIAL CFD SOLVER

by

Miroslav P. PAJČIN, Aleksandar M. SIMONOVIĆ, Toni D. IVANOV*, Dragan M. KOMAROV, and Slobodan N. STUPAR

Department of Aerospace Engineering, Faculty of Mechanical Engineering,
University of Belgrade, Belgrade, Serbia

Original scientific paper
https://doi.org/10.2298/TSCI160518198P

Computational fluid dynamics computations for two hypersonic flow cases using the commercial ANSYS FLUENT 16.2 CFD software were done. In this paper, an internal and external hypersonic flow cases were considered and analysis of the hypersonic flow using different turbulence viscosity models available in ANSYS FLUENT 16.2 as well as the laminar viscosity model were done. The obtained results were after compared and commented upon.

Key words: *computational aerodynamics, turbulence model, hypersonic flow, FLUENT*

Introduction

Space vehicles during reentry experience extreme thermal and aerodynamic loading due to the hypersonic reentry velocity. Also in the recent years there has been a renewed interest and increased effort in development of hypersonic vehicles and hypersonic propulsion. Some of the more popular projects in this field are the Darpa Falcon HTV-2, ESA IXV and DF-ZF. Having in mind that experimental investigation of hypersonic phenomena is very expensive there is an ongoing demand for quality and reliable computational methods for determining aerodynamic and thermodynamic loads.

Hypersonic turbulence modeling is an issue on which many researchers have been working over the years [1-6]. In some cases the assumption of laminar flow can be sufficient but more often it cannot accurately predict surface heat flow and local friction. The need for good turbulence model is even more apparent if it is known that turbulent thermal loads may be 3 times larger than the laminar ones [6]. There are various modifications of the Reynolds--averaged Navier-Stokes (RANS) equation turbulence models adapted for hypersonic flows [7]. Recently researchers have started developing higher order difference schemes codes for hypersonic flows in order to better capture the strong compressibility and shock boundary layer interactions [8, 9].

A progress has been made regarding direct numerical simulation of the Navier--Stokes equations (DNS) for hypersonic flows as well as the large eddy simulation (LES) and

* Corresponding author, e-mail: tivanov@mas.bg.ac.rs

detached eddy simulation (DES) but these are still mostly limited to fundamental studies because of the high computational cost [9, 10].

Most authors use in-house software for hypersonic flow analysis of compression ramps or reentry vehicles, *etc*. Commercial software tools are being constantly improved in regards of hypersonic flow analysis. In this paper the ANSYS FLUENT 16.2.0 CFD software tool was used for analysis of two different hypersonic flow cases. An internal flow and an external flow case analysis were done. The first case was considered as steady 2-D and the second as steady axisymmetric flow while three different standard turbulence viscosity models as well as the laminar viscosity model were considered.

Mathematical and numerical background

The governing equations of continuity, momentum, energy and species transport are solved as a set or vector of equations using the finite volume method and the system of governing equations for a single component fluid is cast in single integral Cartesian form for an arbitrary control volume V with differential surface area dA:

$$\frac{\partial}{\partial t}\int_V W\mathrm{d}V + \oint (F-G)\mathrm{d}A = \int_V \vec{\mathrm{H}}\mathrm{d}V \tag{1}$$

where vector $\vec{\mathrm{H}}$ contains user defined source terms if there are any and W, G, and F are:

$$W = \begin{Bmatrix} \rho \\ \rho u \\ \rho v \\ \rho w \\ \rho E \end{Bmatrix},\quad F = \begin{Bmatrix} \rho v \\ \rho vu + p\hat{i} \\ \rho vv + p\hat{j} \\ \rho vw + p\hat{k} \\ \rho vE + pv \end{Bmatrix},\quad G = \begin{Bmatrix} 0 \\ \tau_{xi} \\ \tau_{yi} \\ \tau_{zi} \\ \tau_{ij}v_j + q \end{Bmatrix} \tag{2}$$

For turbulent flows based on Reynolds-averaged Navier-Stokes equations additional transport equations are needed in order to close the system of equations and determine the Reynolds stresses. Boussinesq hypothesis to relate the Reynolds stresses to the mean velocity gradients was used:

$$-\rho\overline{u_i'u_j'} = \mu_t\left(\frac{\partial u_i}{\partial x_j} + \frac{\partial u_j}{\partial x_i}\right) - \frac{2}{3}\left(\rho k + \mu_t\frac{\partial u_k}{\partial x_k}\right)\delta_{ij} \tag{3}$$

The governing equations for continuity, momentum and energy were solved using the density-based solver with implicit linearization of the governing equations. The governing equations are solved simultaneously, that is, they are coupled together while additional transport equations such as turbulence are solved sequentially or segregated from the coupled set. The first and second order upwind discretization schemes were used and for the derivative and gradient evaluation the least squares cell-based gradient evaluation method was used.

The Roe Flux-Difference Splitting (Roe-FDS) scheme and the Advection Upstream Splitting Method (AUSM+) scheme for computing the convective fluxes were considered and it was found that the AUSM+ scheme allows around 40% faster convergence of the solution. Having this in mind and the fact that the AUSM+ is considered free of carbuncle phenomena, this scheme was chosen for the analysis in this paper.

More detailed information about the mathematical and numerical background can be found in [11, 12].

Turbulence models

Four turbulent viscosity models were used: the one equation Spalart-Allmaras, the two equation standard k-ω as well as k-ω SST and the three equation k-kl-ω model. All of these models use the Boussinesq hypothesis which assumes that the turbulent viscosity μ_t is an isotropic scalar quantity.

Spalart-Allmaras (SA) turbulence model

The Spalart-Allmaras model uses one equation to solve the kinematic eddy viscosity. The transport equation for the modified turbulent viscosity $\tilde{\nu}$ is:

$$\frac{\partial}{\partial t}(\rho\tilde{\nu}) + \frac{\partial}{\partial x_i}(\rho\tilde{\nu}u_i) = G_\nu + \frac{1}{\sigma_{\tilde{\nu}}}\left\{\frac{\partial}{\partial x_j}\left[(\mu+\rho\tilde{\nu})\frac{\partial\tilde{\nu}}{\partial x_j}\right] + C_{b2}\rho\left(\frac{\partial\tilde{\nu}}{\partial x_j}\right)^2\right\} - Y_\nu + S_{\tilde{\nu}} \tag{4}$$

In eq. (4) the turbulent viscosity is $\mu_t = \rho\tilde{\nu}f_{\nu 1}$ where the viscous damping function is given as:

$$f_{\nu 1} = \frac{\chi^3}{\chi^3 + C_{\nu 1}{}^3} \quad \text{and} \quad \chi \equiv \frac{\tilde{\nu}}{\nu} \tag{5}$$

The production term is $G_\nu = C_{b1}\rho\tilde{S}\tilde{\nu}$ with $\tilde{S} \equiv S + \tilde{\nu}/k^2d^2 f_{\nu 2}$ and $f_{\nu 2} = 1-\chi/(1+\chi f_{\nu 1})$.

In Ansys FLUENT 16.2 both vorticity and strain tensors are taken into consideration when calculating S:

$$S \equiv |\Omega_{ij}| + C_{prod}\min\left(0, |S_{ij}| - |\Omega_{ij}|\right) \tag{6}$$

where $C_{prod} = 2.0$, $|\Omega_{ij}| \equiv (2\Omega_{ij}\Omega_{ij})^{1/2}$ and and the mean strain rate S_{ij} is defined as:

$$S_{ij} \equiv \frac{1}{2}\left(\frac{\partial u_j}{\partial x_i} + \frac{\partial u_i}{\partial x_j}\right) \tag{7}$$

The destruction term is modeled as:

$$Y_\nu = C_{w1}\rho f_w\left(\frac{\tilde{\nu}}{d}\right)^2 \tag{8}$$

where $f_w = g[(1 + C_{w3}{}^6)/(g^6 + C_{w3}{}^6)]^{1/6}$, $g = r + C_{w2}(r^6 - r)$ and $r \equiv \tilde{\nu}/(\tilde{S}k^2d^2)$.

The model constants have the default values: $C_{b1} = 0.1355$, $C_{b2} = 0.622$, $C_{\nu 1} = 7.1$, $\sigma_{\tilde{\nu}} = 2/3$, $C_{w2} = 0.3$, $C_{w3} = 2.0$, $k = 0.4187$, and $C_{w1} = C_{b1}/k^2 + (1+C_{b2})/\sigma_{\tilde{\nu}}$.

The turbulent heat transport is modeled with the Reynolds analogy to turbulent momentum transfer. The energy equation is represented as:

$$\frac{\partial}{\partial t}(\rho E) + \frac{\partial}{\partial x_i}\left[u_i(\rho E + p)\right] = \frac{\partial}{\partial x_j}\left[\left(k + \frac{c_p\mu_t}{\mathrm{Pr}_t}\right)\frac{\partial T}{\partial x_j} + u_i(\tau_{ij})_{eff}\right] + S_h \tag{9}$$

where k is the thermal conductivity, E − the total energy, and $(\tau_{ij})_{\mathrm{eff}}$ − the deviatoric stress tensor in the form:

$$\left(\tau_{ij}\right)_{eff} = \mu_{eff}\left(\frac{\partial u_j}{\partial x_i} + \frac{\partial u_i}{\partial x_j}\right) - \frac{2}{3}\mu_{eff}\frac{\partial u_k}{\partial x_k}\delta_{ij} \tag{10}$$

Shear-stress transport k-ω (SST k-ω) turbulence model

The SST *k-ω* model uses two equations to solve the kinematic eddy viscosity. The transport equations for the SST *k-ω* model are:

$$\frac{\partial}{\partial t}(\rho k) + \frac{\partial}{\partial x_i}(\rho k u_i) = \frac{\partial}{\partial x_j}\left(\Gamma_k \frac{\partial k}{\partial x_j}\right) + G_k - Y_k + S_k \tag{11}$$

$$\frac{\partial}{\partial t}(\rho \omega) + \frac{\partial}{\partial x_j}(\rho \omega u_i) = \frac{\partial}{\partial x_j}\left(\Gamma_\omega \frac{\partial \omega}{\partial x_j}\right) + G_\omega - Y_\omega + D_\omega + S_\omega \tag{12}$$

In these equations the term G_k represents the production of turbulence kinetic energy due to mean velocity gradients, G_ω represents the generation of ω, Y_ω and Y_k represent the dissipation of k and ω due to turbulence, S_k and S_ω are user-defined source terms while Γ_k and represent Γ_ω the effective diffusivity of k and ω. The effective diffusivities of k and ω are given by:

$$\Gamma_k = \mu + \frac{\mu_t}{\sigma_k} \quad \text{and} \quad \Gamma_\omega = \mu + \frac{\mu_t}{\sigma_\omega} \tag{13}$$

The Prandtl numbers of k and ω, σ_k and σ_ω, are given: $\sigma_k = 1/(F_1/\sigma_{k1} + (1 - F_1)/\sigma_{k2})$ and $\sigma_\omega = 1/(F_1/\sigma_{\omega 1} + (1 - F_1)/\sigma_{\omega 2})$. F_1 is a blending function and is calculated as $F_1 = \tanh(\Phi_1^4)$ where:

$$\Phi_1 = \min\left[\max\left(\frac{\sqrt{k}}{0.09\omega y}, \frac{500\mu}{\rho y^2 \omega}\right), \frac{4\rho k}{\sigma_{\omega,2} D_\omega^+ y^2}\right] \tag{14}$$

$$D_\omega^+ = \max\left[2\rho\frac{1}{\sigma_{\omega,2}}\frac{1}{\omega}\frac{\partial \omega}{\partial x_j}, 10^{-10}\right] \tag{15}$$

In the SST *k-ω* model a limiter to the formulation of the turbulent viscosity is added in order to stop the over prediction of the eddy-viscosity. The turbulent viscosity μ_t is defined as $\mu_t = \alpha^* \rho k/\omega$ where α^* is a low-Reynolds correction and in the high-Reynolds number form has a value of $\alpha^* = 1$:

$$\mu_t = \frac{\rho k}{\omega}\frac{1}{\max\left[\frac{1}{\alpha^*}, \frac{SF_2}{a_1 \omega}\right]} \tag{16}$$

where α^* is a low-Reynolds correction and in the high-Reynolds number form has a value of $\alpha^* = 1$, while the blending function F_2 is defined as $F_2 = \tanh(\Phi_2^2)$ where:

$$\Phi_2 = \max\left[2\frac{\sqrt{k}}{0.09\omega y}, \frac{500\mu}{\rho y^2 \omega}\right] \tag{17}$$

The production of turbulence kinetic energy is $G_k = \mu_t S^2$ where S is the modulus of the mean rate-of-strain tensor defined as in eq. (7). The production of ω is given by $G_\omega = (\alpha\alpha^*/\nu_t)G_k$. The dissipation of turbulence kinetic energy is represented as:

$$Y_k = \rho\beta^* k\omega \tag{18}$$

while the dissipation of the specific dissipation rate is:

$$Y_\omega = \rho\beta\omega^2 \tag{19}$$

where $\beta_i = F_1\beta_{i,1} + (1 - F_1)\beta_{i,2}$. Because this method is based on the standard k-ω and the standard k-ε models a cross-diffusion modification term D_ω is introduced in order to blend the two models together. D_ω is defined as:

$$D_\omega = 2(1-F_1)\rho\frac{1}{\omega\sigma_{\omega,2}}\frac{\partial k}{\partial x_j}\frac{\partial\omega}{\partial x_j} \tag{20}$$

The k-kl-ω transition turbulence model

The k-kl-ω transition model can be used in order to effectively address the transition of the boundary layer from a laminar to turbulent regime. It is a three equation eddy viscosity model which includes transport equations for turbulent kinetic energy (k_T), laminar kinetic energy (k_L), and the inverse turbulent time scale (ω).

$$\frac{Dk_T}{Dt} = P_{K_T} + R + R_{NAT} - \omega k_T - D_T + \frac{\partial}{\partial x_j}\left[\left(\nu + \frac{\alpha_T}{\alpha_K}\right)\frac{\partial k_T}{\partial x_j}\right] \tag{21}$$

$$\frac{Dk_L}{Dt} = P_{K_L} - R - R_{NAT} - D_L + \frac{\partial}{\partial x_j}\left[\nu\frac{\partial k_L}{\partial x_j}\right] \tag{22}$$

$$\frac{D\omega}{Dt} = C_{\omega 1}\frac{\omega}{k_T}P_{K_T} + \left(\frac{C_{\omega R}}{f_W} - 1\right)\frac{\omega}{k_T}(R + R_{NAT}) - C_{\omega 2}\omega^2 + C_{\omega 3}f_\omega{}^2\frac{\sqrt{k_T}}{d^3} + \frac{\partial}{\partial x_j}\left[\left(\nu + \frac{\alpha_T}{\alpha_\omega}\right)\frac{\partial\omega}{\partial x_j}\right] \tag{23}$$

The turbulent and laminar fluctuations on the mean flow and energy equations are included via the eddy viscosity and the total thermal diffusivity:

$$-\overline{u_i' u_j'} = \nu_{TOT}\left(\frac{\partial U_i}{\partial x_j} + \frac{\partial U_j}{\partial x_i}\right) - \frac{2}{3}k_{TOT}\delta_{ij} \tag{24}$$

The effective length is $\lambda_{eff} = \min(C_\lambda d, \lambda_T)$ where $\lambda_T = k^{1/2}/\omega$ is the turbulent length scale. The small scale and large scale energy are defined in eq. (25) and eq. (26), respectively:

$$k_{T,s} = f_{SS} f_W k_T \quad \text{where} \quad f_W = \frac{\lambda_{eff}}{\lambda_T} \quad \text{and} \quad f_{SS} = \exp\left[-\left(\frac{C_{SS}\nu\Omega}{k_T}\right)^2\right] \tag{25}$$

$$k_{T,l} = k_T - k_{T,s} \tag{26}$$

The turbulence production term P_{kT} generated by turbulent fluctuations and the production of laminar kinetic energy P_{kL} by large scale turbulent fluctuations are computed as:

$$P_{k_T} = \nu_{T,s} S^2 \quad \text{and} \quad P_{k_L} = \nu_{T,l} S^2 \tag{27}$$

The small scale and large scale turbulent viscosity are given by eq. (28) and eq. (29), respectively:

$$\nu_{T,s} = f_\nu f_{INT} C_\mu \sqrt{k_{T,s}}\, \lambda_{eff} \tag{28}$$

$$\nu_{T,l} = \min\left\{ \nu^*_{T,l}, \frac{0.5\left(k_L + {}_{T,l}\right)}{S} \right\} \tag{29}$$

The total eddy diffusivity $\alpha_{\theta TOT}$ and turbulent scalar diffusivity α_T are defined as:

$$\alpha_{\theta,TOT} = f_W \left(\frac{k_T}{k_{TOT}}\right) \frac{\nu_{T,s}}{\mathrm{Pr}_\theta} + \left(1 - f_W\right) C_{\alpha,\theta} \sqrt{k_T}\, \lambda_{eff} \tag{28}$$

$$\alpha_T = f_V C_{\mu,std} \sqrt{k_{T,s}}\, \lambda_{eff} \tag{29}$$

All other equations considering the turbulence models such as breakdown of turbulence, damping functions, near wall dissipation, *etc*. as well as the model constants that are not given here can be found in [11].

Analysis and results

Shock wave boundary interaction in internal hypersonic flow

In this case the shock wave/turbulent boundary layer interaction at hypersonic velocity is analyzed. A 10 degree angle on 300 mm long shock generator plate was used to create an oblique shock impinging on an opposite 500 mm long flat plate, fig. 1.

The hypersonic flow was considered as 2-D steady. Sensitivity analysis using few different grids was performed. Three different structured multiblock planar grids with quadrilateral cells as well as an unstructured grid consisted of triangular cells and inflated prisms near the wall boundaries were considered. The grids characteristics are given in tab. 1.

The coarse structured grid and the unstructured grid were adapted in the shock wave interaction and flow recirculation region and around the shock waves using the FLUENT adapt options. The dimensionless wall distance was set to $y^+ < 1$ for all grids.

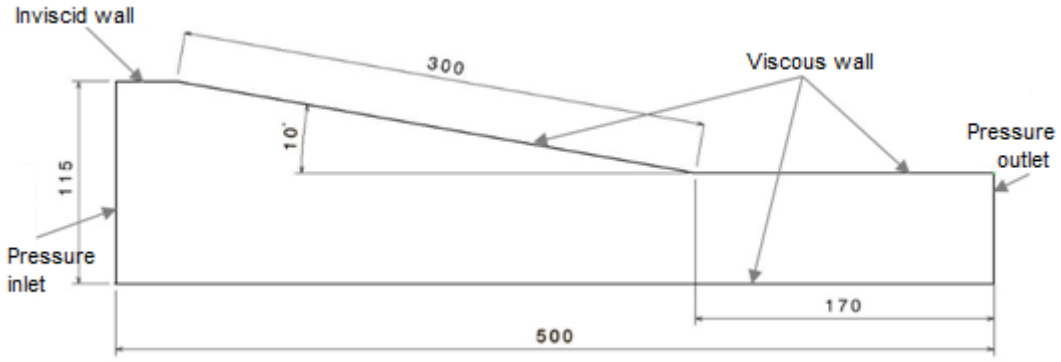

Figure 1. Model geometry

Table 1. Grid characteristics

Grid	Number of cells	After adaptation	First cell distance	Cell ratio
Structured coarse	10858	28160	0.005	1.1
Structured medium	58646	–	0.005	1.1
Structured fine	154380	–	0.005	1.1
Unstructured	35731	48238	0.002 (20 prism layers)	1.2

The boundary conditions were set as to obtain freestream condition values given in tab. 2. These values correspond with the experimental investigations performed in the German Aerospace Center (DLR) given in [13].

Table 2. Freestream conditions

Mach number	Pressure [Pa]	Total pressure [Pa]	Total temperature [K]	Turbulent intensity [%]	Turbulent viscosity ratio
5	4012	2122516	410.7	0.1	10

During the calculations the gas was considered as ideal and the viscosity was calculated using the Sutherland equation. The density based implicit formulation solver was used. In order to accelerate convergence the hypersonic solution steering option was selected and full multigrid initialization with 3 multigrid levels was used. The first iterations were done using the first order spatial discretization scheme after which the second order spatial discretization scheme was used.

The skin friction coefficient C_f of the lower surface obtained with the S-A turbulence model for the six grids in tab. 1 in comparison with the experimental results given in [13] is shown in fig. 2. It can be seen that almost all grids give reasonable results in compari-

son to the experiment with the finest being the best as is to be expected. The results further presented in this paper are obtained using the finest structured grid.

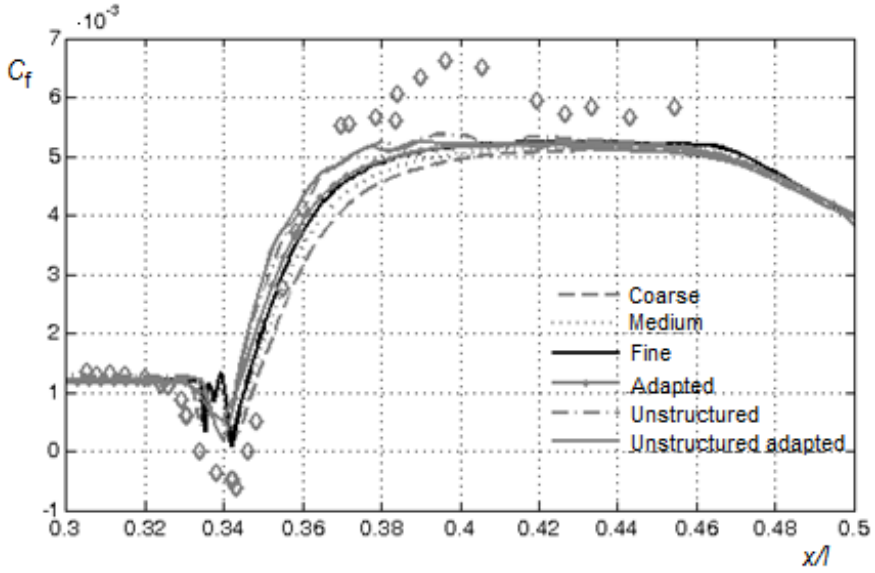

Figure 2. Skin friction coefficient obtained with S-A for different grids

In fig. 3 the skin friction coefficient obtained with different turbulence models is shown. It can be seen that all of the turbulence models capture the shock wave/boundary layer interaction on the lower wall with the S-A and standard *k-ω* being the best and the SST *k-ω* the worst in comparison to experimental data. It can also be noticed that all turbulence models underestimate the skin friction coefficient after the separation region.

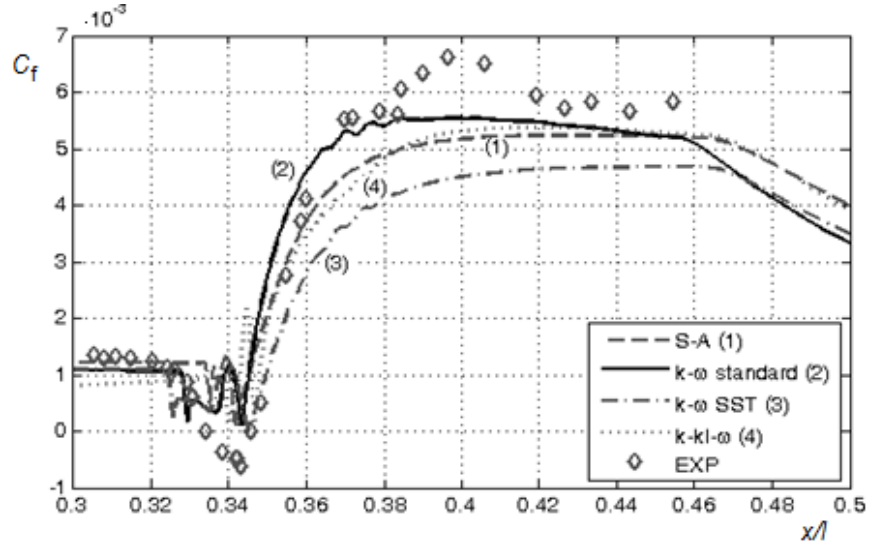

Figure 3. Skin friction coefficient obtained with different turbulence models

In fig. 4 the axial velocity profiles in the x-direction in the boundary layer compared with the experimental results for four different locations along the lower surface are shown.

It can be seen that the S-A and standard *k-ω* turbulence models give excellent concurrence with the experimental data while the SST *k-ω* and *k-kl-ω* models were unable to correctly predict the velocity profile in such that SST *k-ω* underestimated and *k-kl-ω* significantly overestimated the velocity near the wall surface.

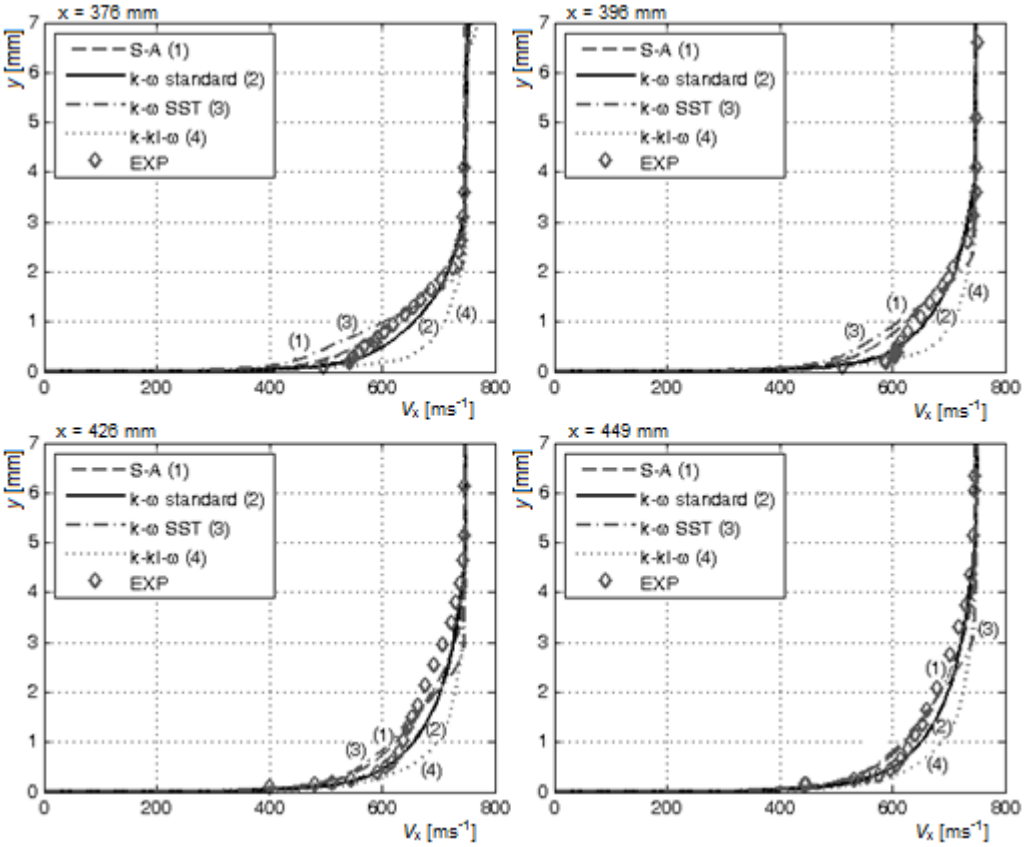

Figure 4. Velocity profiles in the boundary layer

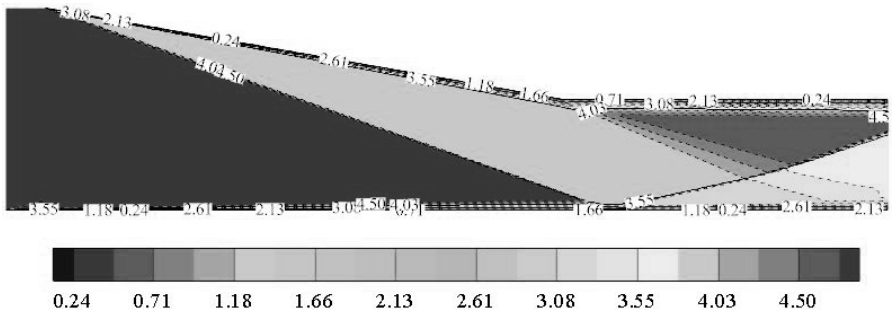

Figure 5. Mach number contours

In fig. 5 the Mach number contours obtained with the S-A turbulence model are shown. The impinging shock wave, the reflected shock, the expansion fan as well as the separation bubble, although small, can be observed. This is in agreement with the shadowgraph given in [13].

Shock wave boundary interaction in internal hypersonic flow

In this case the hypersonic flow over the standard ballistic correlation model HB-2 which is essentially a blunt cone-cylinder with a flare was considered, fig. 6. This geometry was proposed by AGARD and STA in the late fifties of the 20th century and the model has been extensively tested over the years.

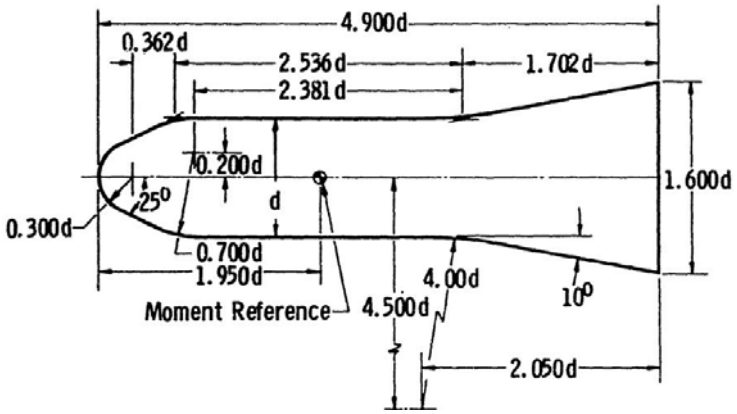

Figure 6. The HB-2 model geometry [14]

Even though the flow over the HB-2 model is generally considered as laminar, at Mach 4 according to Gray [14] the boundary layer is turbulent therefore analysis using the S-A, SST k-ω and k-kl-ω turbulence models were also made in order to see if any difference in the results is going to be seen especially in the cylinder-flare transition zone.

The HB-2 was modeled as 2-D axisymmetric and the hypersonic flow was considered as steady. A coarser grid, fig. 7, consisting of 26966 cells which was later refined in the cylinder-flare junction region using the adapt option and a finer grid consisting of 143001 cells were considered. The coarse grid was stretched in the longitudinal direction in the region with relatively low gradients while the finer one was uniform. Computations were done with boundary conditions considered as pressure farfield as well as pressure inlet-pressure outlet. It has been concluded that the pressure inlet-pressure outlet boundary condition is more stable while the pressure farfield boundary condition has difficulties and is more slowly converging.

Values of Mach number, pressure, total pressure and total temperature prescribed at domain boundaries are given in tab. 3 and are chosen according to the experimental investigations done by Gray [14]. The gas was considered as ideal with viscosity calculated by the Sutherland equation. The density implicit based formulation as well as the solution steering option and the FMG initialization were used. As a convergence criterion for the solution the scaled residuals were set to be less than 10^{-4} and change in mass flow rate was in the order 10^{-2} or less than 0.01% of the overall mass flow rate. In order to ensure convergence the Courant number in the solution steering was allowed to have values between 0.1 and 0.8.

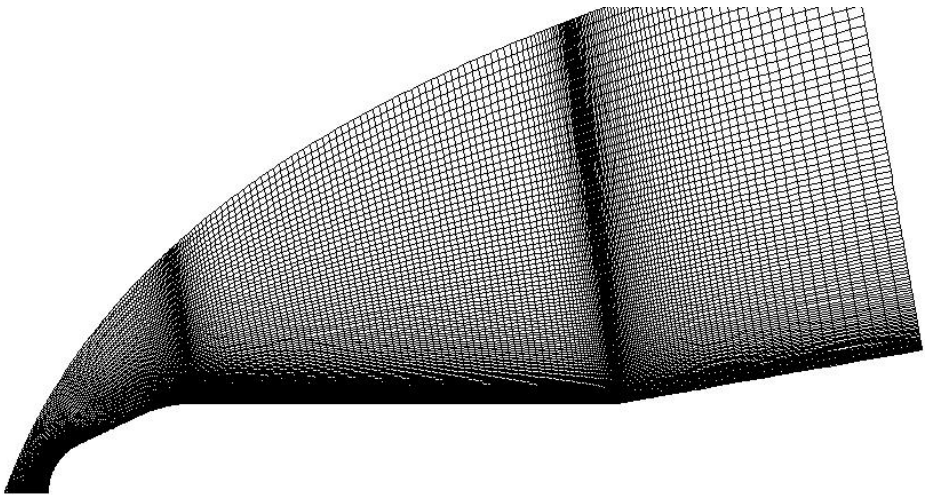

Figure 7. The HB-2 computational grid

Table 3. Freestream conditions for the HB-2 model

Mach number	Pressure [Pa]	Total pressure [Pa]	Total temperature [K]
5	1142.86	604118	600
4	1142.86	173526	600

In fig. 8 the pressure ratio along the HB-2 model wall for the Mach 5 freestream condition is shown. Only the laminar viscosity and *k-kl-ω* models were able to capture the creation of a laminar bubble in the cylinder-flare junction. All grids were able to capture the separation and reattachment points with the denser one being the best in comparison to experimental data. Further refinement of the grid did not improve the results so the fine one was used for all analysis. It should be noted that increasing the number of cells makes the solution somewhat locally unstable and it was necessary to limit the Courant number to values bellow 0.8 in the hypersonic solution steering in order for the solution to converge.

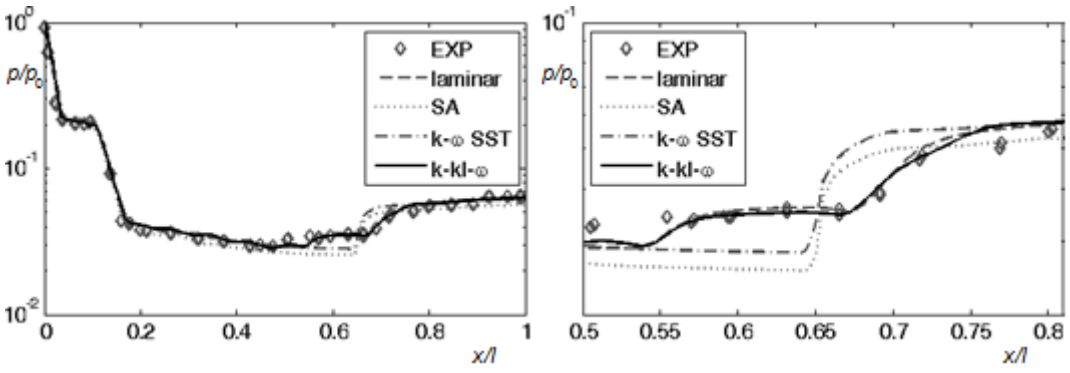

Figure 8. Pressure ratio along the HB-2 model

In fig. 9(a) the pressure ratio for the Mach 4 freestream condition computed with the fine grid as well as a comparison between the laminar, S-A, *k-ω* SST and *k-kl-ω* viscosity models with the experimental data is shown. As in the previous case only the laminar and the *k-kl-ω* models were able to capture the boundary layer developments in the cylinder-flare junction region. In fig. 9(b) the skin friction coefficients are shown. Unfortunately there were no experimental data for the skin friction coefficient available to authors. In fig. 10 the Mach number contours around the Mach 5 freestream condition case obtained with the laminar viscosity model and the fine grid are shown.

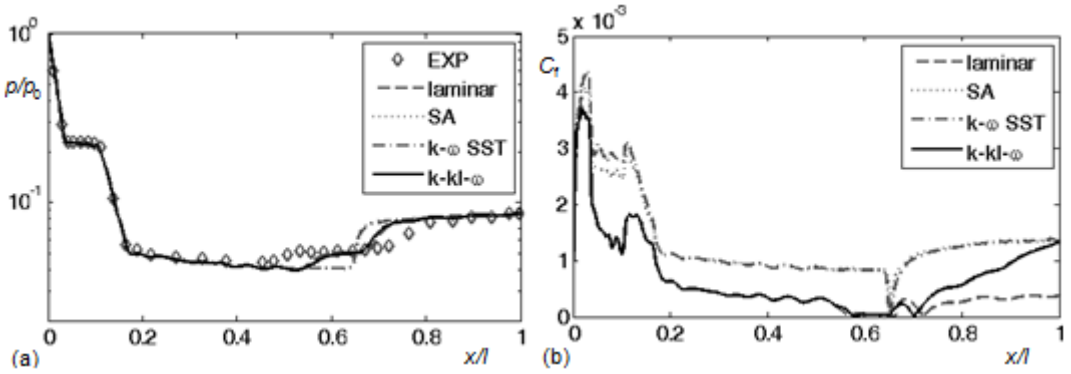

Figure 9. Pressure ratio (a) and skin friction coefficient (b)

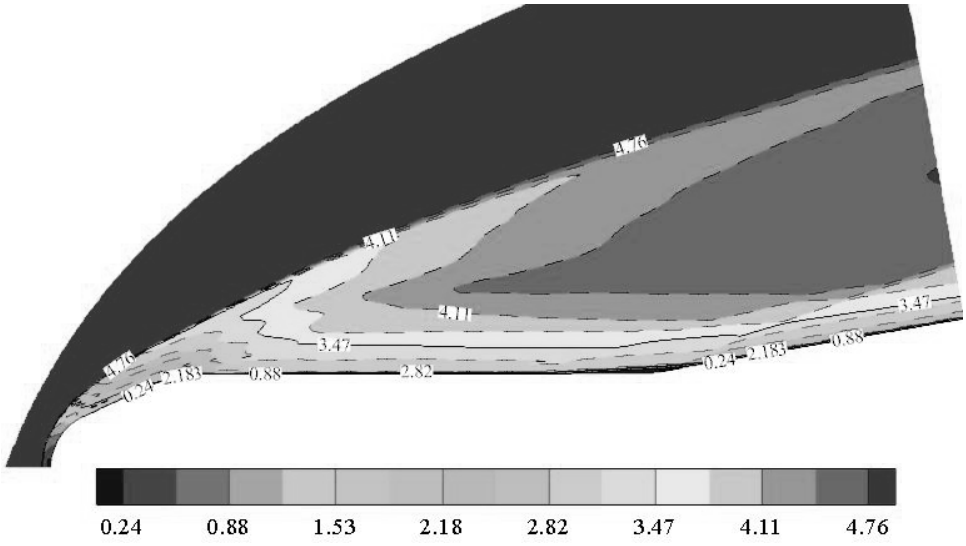

Figure 10. Mach number contours

Conclusions

Numerical analysis of the hypersonic flow in two different cases using the Ansys FLUENT 16.2 commercial software were done. The impinging shock wave boundary interaction was analysed in the first case. All turbulence models gave reasonably good results

with the standard k-ω model being the best in comparison with the experimental data. Grid sensitivity study was done and it was found that in order to ensure convergence, especially with the finer grids, the Courant number in the hypersonic solution steering needed to be limited to values lower than 0.6.

In the case of the external flow over the standard ballistic HB-2 model only the laminar and k-kl-ω viscosity models managed to capture the recirculation flow in the cylinder-flare transition area which was to be expected having in mind that a laminar bubble is formed in that region. The reattachment point is well captured comparing to the experiment results while the total length is smaller than that in the experiment.

Acknowledgment

The research work is funded by Ministry of Education, Science, and Technological Development of Republic of Serbia through Technological Development Project no. 35035.

References

[1] Marvin, J. G., Coakley, T. J., Turbulence Modeling for Hypersonic Flows, Technical Memorandum No. 101079, Ames Research Center, Moffett Field, Cal., USA, 1989
[2] Smits, J. A., *et al*., Current Status of Basic Research in Hypersonic Turbulence, *Proceedings*, 39th AIAA Fluid Dynamics Conference and Exhibit, Orlando, Fla., USA, 2009, paper 2009-151
[3] Roy, J. C., Blottner, G. F., Review and Assessment of Turbulence Models for Hypersonic Flows: 2D/Axisymmetric Cases, *Proceedings*, 44th AIAA Aerospace Sciences Meeting and Exhibit, 2006, Reno, Nev., USA, AIAA 2006-713, pp. 1-99
[4] Savio, E., Maciel, G., Comparison of Several Turbulence Models as Applied to Hypersonic Flows in 2D – Part II, *AASCIT J. of Physics*, *1* (2015), 4, pp. 275-287
[5] Roy, J. C., Blottner, G. F., Methodology for Turbulence Model Validation: Application to Hypersonic Flows, *J. of Spacecraft and Rockets*, *40* (2003), 3, pp. 313-325
[6] Longo, J. M. A., *et al*., The Challenge of Modeling High Speed Flows, *Proceedings*, 6th EUROSIM Congress on Modelling and Simulation, Ljubljana, Slovenia, 2007
[7] Liang, W., Song, F., Modeling Flow Transition in a Hypersonic Boundary Layer with Reynolds-Averaged Navier-Stokes Approach, *Science in China Series G: Physics, Mechanics & Astronomy*, *52* (2009), 5, pp. 768-774
[8] Tissera, S., Assesment of High-Resolution Methods in Hypersonic Real-Gas Flows, Ph. D. thesis, Cranfield University, Cranfield, UK, 2010
[9] Wu, M., Martin, P. M., Direct Numerical Simulation of Supersonic Turbulent Boundary Layer over a Compression Ramp, *AIAA Journal*, *45* (2007), 4, pp. 879-889
[10] Loginov, S. M., Large-Eddy Simulation of Shock Wave/Turbulent Boundary Later Interaction, Ph. D. thesis, Technical University of Munich, Munich, Germany, 2006
[11] ***, ANSYS FLUENT Theory Guide, ANSYS, Inc., Canonsburg, Penn., USA, 2015
[12] ***, ANSYS FLUENT User Guide, ANSYS, Inc., Canonsburg, Penn., USA, 2015
[13] Schulein, E., *et al*., Documentation of Two-Dimensional Impinging Shock/Turbulent Boundary Layer Interaction Flow, Technical Report IB 223-96 A 49, German Aerospace Center (DLR), Gottingen, Germany, 1996
[14] Gray, D. J., Summary Report on Aerodynamic Characteristics of Standard Models HB-1 and HB-2, Technical Report No. AEDC-TDR-64-137, Von Karman Dynamics Facility, 1964

Paper submitted: May 18, 2016
Paper revised: June 29, 2016
Paper accepted: July 4, 2016